

# Quantifying microbubble clustering in turbulent flow from single-point measurements

Enrico Calzavarini,<sup>1,a)</sup> Thomas H. van den Berg,<sup>1</sup> Federico Toschi,<sup>2</sup> and Detlef Lohse<sup>1,b)</sup>

<sup>1</sup>Department of Applied Physics, JMBC Burgers Center for Fluid Dynamics, and IMPACT Institute, University of Twente, 7500 AE Enschede, The Netherlands

<sup>2</sup>IAC-CNR, Istituto per le Applicazioni del Calcolo, Viale del Policlinico 137, I-00161 Roma, Italy and INFN, via Saragat 1, I-44100 Ferrara, Italy

(Received 24 September 2007; accepted 28 December 2007; published online 30 April 2008)

Single-point hot-wire measurements in the bulk of a turbulent channel have been performed in order to detect and quantify the phenomenon of preferential bubble accumulation. We show that statistical analysis of the bubble-probe colliding-time series can give a robust method for investigation of clustering in the bulk regions of a turbulent flow where, due to the opacity of the flow, no imaging technique can be employed. We demonstrate that microbubbles ( $R_0 \approx 100 \mu\text{m}$ ) in a developed turbulent flow, where the Kolmogorov-length scale is  $\eta \approx R_0$ , display preferential concentration in small scale structures with a typical statistical signature ranging from the dissipative range,  $\mathcal{O}(\eta)$ , up to the low inertial range  $\mathcal{O}(100\eta)$ . A comparison to Eulerian–Lagrangian numerical simulations is also presented to further support our proposed way to characterize clustering from temporal time series at a fixed position. © 2008 American Institute of Physics. [DOI: 10.1063/1.2911036]

## I. INTRODUCTION

The phenomenon of preferential concentration of small particles and bubbles in turbulent flows attracted much attention in recent years, from experimental works,<sup>1–6</sup> to numerical investigations,<sup>7–18</sup> and theoretical developments.<sup>19</sup> The preferential accumulation is an inertial effect. Particles heavier than the fluid are on average ejected from vortices, while light buoyant particles tend to accumulate in high vorticity regions. Small air bubbles in water [below 1 mm, typical Reynolds number of order  $\mathcal{O}(1)$ ] can be regarded as a particular kind of nondeformable light spherical particles with density negligibly small compared to the fluid one. In fact, in this size range, shape oscillations or deformations, and wake induced effect can be reasonably neglected. Strong preferential bubble accumulation in core vortex regions is therefore expected according to the inertia mechanism, and indeed observed experimentally<sup>2</sup> and numerically.<sup>20,21</sup> Next to the added mass force and gravity also drag and lift forces can affect the clustering. Moreover, the coupling of the disperse phase to the fluid flow (*two-way* coupling) and the finite-size effect of particle-particle interaction (*four-way* coupling) may also result in non-negligible factors of perturbation for preferential concentration of particles and bubbles in highly turbulent flows.

Both the lift force, the two-way coupling, and the four-way coupling are notoriously difficult to model in numerical simulations and a validation of the models against numerical simulations is crucial. However, experimental measurements on bubbly laden turbulent flows are challenging, as even at very low void fractions ( $\sim 1\%$  in volume) the fluid is completely opaque and difficult to access with external optical methods, especially in the bulk region of the flow. To experi-

mentally explore the bubble clustering in the bulk at high void fraction one therefore has to fall back on *intrusive* hot-wire anemometer measurements. Such measurements had earlier been employed to determine the modification of turbulent spectra through bubbles.<sup>22–24</sup> For the calculation of the velocity spectra bubbles hitting the probe had first to be identified in the hot-wire signals<sup>25,26</sup> and then filtered out. In the present paper, we employ the very same hot-wire time series to obtain information on the bubble clustering in the turbulent flow. An alternative method to obtain local information on the bubble distribution may be phase doppler particle analyzers.<sup>27</sup>

One could object that measurement from one fixed point in space are too intrusive because they can destroy the clusters, or that they are ineffective in extracting features of the bubble trapping in turbulent vortical structures. The aim of this paper is to demonstrate that this is not the case, when using appropriate statistical indicators for the analysis of series of bubble colliding times on the hot-wire probe. We show that it is possible to detect and quantify the microbubble clustering from a one-point measurement setup. We compare experimental findings with results from numerical simulations based on Eulerian–Lagrangian approach. Due to limitations that we will discuss later, only a qualitative agreement among numerics and experiments is expected. Nevertheless, we show how this comparison is helpful in clarifying the trend in the clustering at changing the turbulent conditions.

## II. DETAILS OF THE EXPERIMENT METHODS

The experimental setup is the Twente water channel, a vertical duct of square cross section with dimension  $200 \times 45 \times 45 \text{ cm}^3$ . We refer to Rensen *et al.*<sup>22</sup> for a detailed description. An array of porous ceramic plates, positioned on

<sup>a)</sup>Electronic mail: enrico.calzavarini@ens-lyon.fr.

<sup>b)</sup>Electronic mail: d.lohse@utwente.nl.

TABLE I. Relevant turbulent scales and bubble characteristics for the two experimental samples analyzed. Fluid turbulent quantities have been estimated from one-dimensional energy spectra. From left to right: integral scale,  $L_0$ , mean velocity,  $U$ , single-component root mean square velocity,  $u'$ , Taylor Reynolds number,  $Re_\lambda$ , large eddy turnover time,  $\tau_{\text{eddy}}$ , dissipative time ( $\tau_\eta$ ) space ( $\eta$ ), and velocity ( $u_\eta$ ) scales, bubble Reynolds number (based on rising velocity in still fluid),  $Re_b$ , bubble-radius and Kolmogorov-length ratio,  $R_0/\eta$ , Stokes number,  $St$ , ratio between terminal velocity in still fluid and dissipative velocity scale,  $g\tau_b/u_\eta$

	$L_0$ (cm)	$U$ (cm/s)	$u'$ (cm/s)	$Re_\lambda$	$\tau_{\text{eddy}}$ (s)	$\tau_\eta$ (ms)	$\eta$ ( $\mu\text{m}$ )	$u_\eta$ (mm/s)	$Re_b$	$R_0/\eta$	$St$	$g\tau_b/u_\eta$
(a)	22.6	19.4	1.88	206	12.0	151.0	388.0	2.57	4.4	0.26	0.007	4.2
(b)	23.1	14.2	1.39	180	16.6	240.0	489.0	2.04	4.4	0.20	0.004	5.3

the top of the channel, is used to generate coflowing small bubbles of average radius,  $R_0 \approx 100 \mu\text{m}$ , as described in Ref. 23. Fluid turbulence is generated by means of an active grid, positioned immediately downstream the bubble injection sites. The typical flow is characterized by a large mean flow,  $U$ , with turbulent fluctuations,  $u' \equiv \langle (u_z(t) - U)^2 \rangle_t^{1/2}$ , of smaller amplitude. The condition  $u'/U \ll 1$  assures that Taylor's frozen-flow hypothesis can be applied. The dissipative Kolmogorov scale measures typically  $\eta = 400 - 500 \mu\text{m}$ , while the Taylor microscale and the integral one, are, respectively,  $\lambda \approx 30\eta$ , and  $L_0 \approx 500\eta$ . The typical bubble size is of the same order, or slightly smaller, than  $\eta$ .

We consider microbubble signals extracted from a hot-film anemometry probe ( $300 \mu\text{m}$  in size) fixed at the center of the channel. Detection of microbubbles is less ambiguous than for large bubbles where probe piercing and breakup events are highly probable.<sup>28</sup> A microbubble hitting the probe produces a signal with a clear spike. The bubble can be identified by thresholding of the velocity time-derivative signal, see Fig. 2 of Ref. 23. This identification procedure leads to the definition of a minimal cutoff time in the capability to detect clustered events, two consecutive bubbles in our records cannot have a separation time smaller than  $\tau = 10^{-2}$  s. Such dead time is mainly linked to the typical response-time of the acquisition setup. Here, we consider two time series of microbubble measurements, i.e., hitting times, selected from a larger database because of their uniformity and relevant statistics. We will refer to them in the following as samples (a) and (b). The first sample (a) has been taken for a 12 h long measurement; it consists of  $N_b = 240\,99$  bubbles with a mean hitting frequency  $f = 0.56 \text{ s}^{-1}$ . The second sample, (b), is a record of 11 h,  $N_b = 111\,94$  and  $f \approx 0.28 \text{ s}^{-1}$ . There are two main differences among the experimental conditions in which the two samples have been recorded, that is the total volume air fraction (called void fraction  $\alpha$ ), and the amplitude of the mean flow and therefore the intensity of turbulence. Case (a) has a void fraction of  $\approx 0.3\%$  and (b) has instead  $\alpha \approx 0.1\%$ . Note that, even at these very small void fractions, the mean number density of bubbles amounts to  $O(10^2)$  per cubic centimeter. This explains the optical opacity of the bulk region of our system. Nevertheless, given the small effect produced by the dispersed bubbly phase on the turbulent cascading mechanism,<sup>23</sup> we consider the discrepancy in  $\alpha$  as irrelevant for the velocity spectra. In contrast, the difference in the forcing amplitude is more important, because it sensibly changes all the relevant scales of turbulence, as summarized in Table I. In particular, this leads to different values for

minimal experimentally detectable scale:  $\Delta r_{\text{min}} \approx 5\eta$  for case (a) and  $\Delta r_{\text{min}} \approx 3\eta$  for (b), where Taylor hypothesis has been used to convert time to space measurements, i.e.,  $\Delta r = \tau U$ . In the following, results of our analysis will be presented by adopting space units made dimensionless by the Kolmogorov scale  $\eta$ . We consider this rescaling more useful for comparison to different experiments and simulations where a mean flow may be absent.

### III. DESCRIPTION OF THE STATISTICAL TOOLS

In this section, we introduce the statistical tests that we will adopt to quantify the clustering. Due to the fact that the experimental recording is a temporal series of events, we have necessarily to focus on a tool capable to identify, from within this one dimensional series, possible signatures of three-dimensional inhomogeneities.

A first way to assess the presence of preferential concentrations in the experimental records is to compute the probability density function (pdf) of the distance,  $\Delta r$ , between two consecutive bubbles. Whether the particles distribute homogeneously in space, their distribution would be a Poissonian distribution and hence the distance between two consecutive bubbles would be given by the well known exponential expression:  $\rho \exp(-\rho \Delta r)$ , where  $\rho = f/U$  is the number of bubbles per unit length (i.e., their density).<sup>29</sup> Due to the presence of turbulence, we expect that, in general, the spatial distribution of the bubbles will differ from a Poissonian distribution: in any case, it is natural to expect that for separation scales large enough the exponential form of the pdf should be recovered. In fact, pairs of successive bubbles with large separations  $\Delta r$ , larger than any structures in the flow, are expected to be uncorrelated, memoryless, events.

Due to the possible accumulation on small scales (clustering of bubbles), the long tail of the pdf may have an exponential decay rate that is different from the global mean,  $\rho$ . The tail of the experimentally measured pdf can be fitted with an exponentially decaying function,  $A \exp(-\rho_h \Delta r)$ , with a rate that we call  $\rho_h$ , where  $h$  stands for homogeneous. In the case of small-scale clustering, we expect  $\rho_h$  to be smaller than  $\rho$ . As an indicator of the fraction of bubbles accumulated in turbulent structures, we use the coefficient  $C \equiv 1 - \rho_h/\rho$ , whose value varies in between 0 and 1.

The test, so far, introduced is useful but only provides an indication on how homogeneously distributed the bubbles are at small scales, while it gives no indication on their possible "large-scale" correlations. Here, we introduce a second, more comprehensive, statistical test particularly convenient

to reveal the scales at which the inhomogeneity develops. The idea is to compute the coarse-grained central moments of the number of bubbles, on a window of variable length  $r$ ,  $\mu_r^p \equiv \langle (n - \langle n \rangle_r)^p \rangle_r$ . The length of the window  $r$  will be the scale at which we study whether the distribution resembles a homogeneous one. We will focus on scale dependent kurtosis and skewness excesses, respectively:  $K(r) \equiv \mu_r^4 / (\mu_r^2)^2 - 3$  and  $S(r) \equiv \mu_r^3 / (\mu_r^2)^{3/2}$ . A random distribution of particles spatially homogeneous with mean density  $\rho$  corresponds to the Poissonian distribution:  $p(n) = \exp(-\rho r) (\rho r)^n (n!)^{-1}$ , where  $r$  is the length of the spatial window and  $n$  is the number of expected events. Therefore, once the particle space rate  $\rho$  is given, the value of any statistical moment can be derived for the corresponding window length  $r$ . A spatially Poissonian distribution of particles implies the functional dependences  $K(r) = (\rho r)^{-1}$  and  $S(r) = (\rho r)^{-1/2}$ . Furthermore, we note that at the smallest scale, when  $r = \Delta r_{\min}$ , we reach the singular limit (shot-noise limit) where for any given space window, we can find none or only one bubble and all statistical moments collapse to the same value. This latter limit, which is by the way coincident with Poisson statistics, represents our minimal detectable scale. We are interested in departures from the shot-noise/random-homogeneous behavior for the statistical observables  $K(r)$  and  $S(r)$ .

#### IV. RESULTS OF THE ANALYSIS ON EXPERIMENTAL DATA

In Fig. 1, we show the computed pdf( $\Delta r$ ) for the two data samples considered. Deviations from global homogeneity are clear if the shape of the histogram is compared to the solid line representing the pdf  $\rho \exp(-\rho \Delta r)$ . These deviations are slightly more pronounced in the more turbulent case (a) as compared to case (b). Nevertheless, one can notice that the pure exponentially decaying behavior, i.e., homogeneity, is recovered from distances of the order of  $\mathcal{O}(100\eta)$  up to the large scales. The dotted line on Fig. 1, which represents the linear fit on the long homogeneous tail in the interval  $[10^3, 2 \times 10^3]\eta$ , and the inset boxes, where the pdf is compensated by the fit, shows this latter feature. The evaluation of the coefficient  $\mathcal{C}$  leads to values for the relative bubbles excess in clusters corresponding to 19% for case (a) ( $\text{Re}_\lambda \approx 206$ ) and 10% for case (b) ( $\text{Re}_\lambda \approx 180$ ), confirming the trend of stronger concentration in flows with stronger turbulence level. In Fig. 2, we show the kurtosis and skewness behavior, evaluated for the two cases (a) and (b), in a comparison with the Poissonian dependence. We observe, in both cases, a clear departure at small scale from the scaling implied by the global homogeneity, which is only recovered at the large scale ( $\geq L_0 \approx 500\eta$ ) where the data points falls roughly parallel to the Poisson line. The departure from the Poisson line, that is noticeable already at the scales immediately above  $\Delta r_{\min}$ , is an indication that bubbles form clusters even at the smallest scale we are able to detect, that is even below  $5\eta$  for case (a) or  $3\eta$  for case (b). We observe that for the less turbulent case, (b), the departure from the homogeneous scaling is less marked. A comparison to synthetic Poisson samples of an equivalent number of bubbles, that we have tried, shows that the available statistics is sufficient to

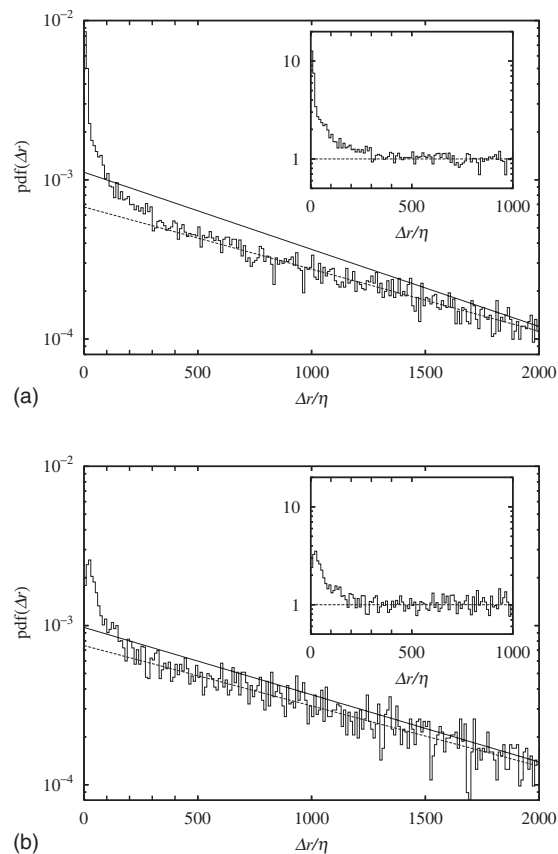


FIG. 1. Probability density function of distance between successive bubbles, pdf( $\Delta r$ ). Exponential behavior,  $\rho e^{-\rho \Delta r}$ , (solid line) and exponential fit,  $A e^{-\rho \Delta r}$ , of the large-scale tail (dashed line) are reported. The inset shows the pdf( $\Delta r$ ) compensated by the fitted large-scale exponential behavior, i.e., the pdf( $\Delta r$ ) divided by  $A e^{-\rho \Delta r}$ .

validate the deviations from the homogeneity discussed so far. Scale dependent deviation from Poisson distribution is an evidence of the fact that the dispersed microbubbles are trapped within the dynamical vortical structures of turbulence. Furthermore, we observe that gravity plays a minor role in this dynamics. In fact, on average the bubbles are swept down by the mean flow and  $g \tau_b / u_\eta \sim \mathcal{O}(1)$  (see Table I), which implies that even the smallest vortical structures of the flow may trap bubbles.<sup>10</sup> Therefore, it is mainly the inertia that drives the bubble accumulation in the flow.

#### V. RESULTS OF THE ANALYSIS ON NUMERICAL DATA

To give further evidence for the robustness of the suggested statistical analysis of the hot-wire time series, we now repeat the very same procedure with numerical simulation data. We employ standard numerical tools already described and discussed in details in Refs. 13 and 14. In short, we integrate Lagrangian pointwise bubbles evolving on the background of an Eulerian turbulent field. The equation for the evolution of the pointwise bubble is the following:

$$\frac{d\mathbf{v}}{dt} = 3 \frac{D\mathbf{u}}{Dt} - \frac{1}{\tau_b} (\mathbf{v} - \mathbf{u}) - 2\mathbf{g} - (\mathbf{v} - \mathbf{u}) \times \boldsymbol{\omega}, \quad (1)$$

where  $\mathbf{u}$  and  $\boldsymbol{\omega}$  are, respectively, the fluid velocity and vorticity computed at the bubble position and constitute a sim-

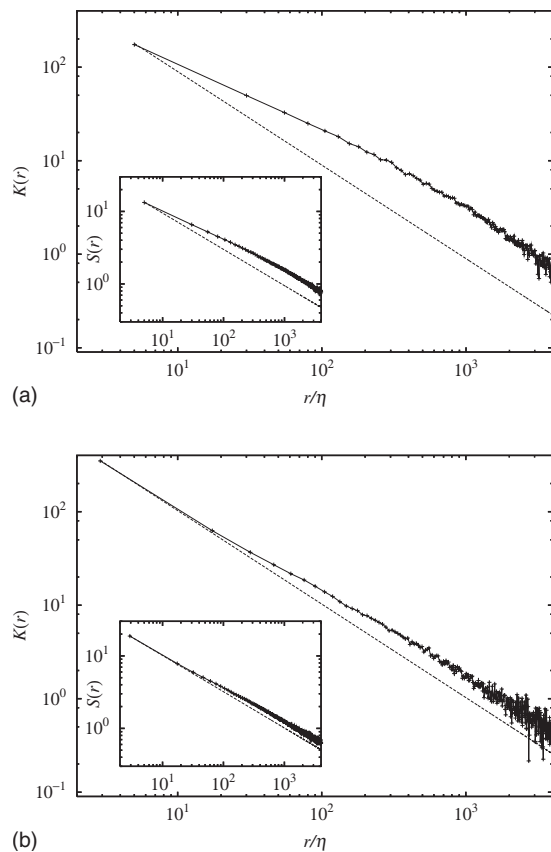


FIG. 2. Scale dependent kurtosis,  $K(r)$ , for cases (a) (top) and (b) (bottom). Dotted lines represent the Poissonian behavior, that is  $K_{(p)}(r) = (\rho r)^{-1}$ . Notice that the Poisson scaling behavior is reached for large  $r$  windows only scaling wise. In the insets, the scale dependent skewness,  $S(r)$ , behavior is shown. Again, the Poissonian relation is drawn  $S_{(p)}(r) = (\rho r)^{-1/2}$  (dotted line).

plified version of the model suggested in Ref. 30 with the addition of the lift term (see Ref. 13). The Eulerian flows is a turbulent homogeneous and isotropic field integrated in a periodic box, of resolution  $128^3$ , seeded approximately with  $10^5$  bubbles, corresponding to a void fraction  $\alpha = 4.5\%$ . Since previous numerical and experimental studies<sup>13,23</sup> have revealed that the effect of bubbles on strong unbounded turbulence is relatively weak, our numerical bubbles are only coupled in one-way mode to the fluid, i.e., bubbles do not affect the fluid phase. The bubble-Reynolds number  $Re_b$  is set to unity and the Stokes number is  $St \ll 1$ . Therefore, the bubble radius is of order  $\eta$ , and the bubble terminal velocity

$v_T = 2g\tau_b$  in still fluid is smaller than the smallest velocity scale  $u_\eta$ . As (and actually even more than) in the experiment, the role of gravity is marginal. In Table II, we report details of the numerical simulations, these are chosen trying to match the experimental numbers. However, we could not reach the same scale separations as in the experiments. In the bottom panel of Table II, we translated the numerical units to their physical equivalent. We note that in the numerics the Stokes number,  $St = \tau_b / \tau_\eta$  which is an indicator of the degree of bubble interaction with turbulence, cannot be as low as in the experiments. To achieve the same,  $St$  would require too much CPU time. For practical reason, the Stokes values adopted in our numerics are roughly one order of magnitude larger than in the experiments, although always much smaller than unity,  $St \ll 1$ . Under this conditions, simple spatial visualization<sup>20</sup> shows strong bubble accumulation in nearly one-dimensional elongated structures in correspondence to high enstrophy regions (identified as vortex filaments). As already stated, our goal is to use the numerics to confirm the behavior of the suggested observables. To this end, we put 128 virtual pointwise probes in the flow and recorded the hitting times of the bubbles, which we give a virtual radius  $R_0$ . The bubble radius is related to the bubble response time  $\tau_b$ , namely,  $R_0 \equiv (9\tau_b \nu)^{1/2}$  when assuming no-slip boundary conditions at the gas-liquid interface.

An important difference between the experiments and the numerics is the mean flow: it is present in the experiment while intrinsically suppressed in the simulations. In the numerical simulations the time is connected to space displacements through the relation  $\Delta R = \Delta t u'$ , where  $u'$  is the root mean square velocity.

The level of turbulence, given the available resolution, has been pushed as high as possible ( $Re_\lambda \approx 90$ ) to obtain a better analogy with the experiment. Also, in the numerical simulations, two cases with different Reynolds numbers are considered, see again Table II.

In Figs. 3 and 4, we show the results of the statistical analysis of clustering from the time series obtained from the numerical virtual probes. These two figures should be compared to the analogous experimental findings already discussed and shown in Figs. 1 and 2. Some qualitative similarities are striking. First, starting from Fig. 3, we observe that deviations from random and homogeneous, i.e., pure exponential behavior, are relevant at small scales. This feature is confirmed by the scale dependent kurtosis and skew-

TABLE II. Relevant turbulent scales and bubble characteristics for the two numerical simulation performed. The top part reports the actual values in numerical units from the simulation, the bottom part shows for comparison the corresponding physical equivalent quantities for air bubbles in water, this is to better appreciate similarities/differences with the experimental conditions of Table I. The values on the bottom part are computed starting from the dimensionless quantities  $Re_\lambda$ ,  $Re_b$ ,  $St$ , and by assuming  $\nu = 10^{-6} \text{ m}^2 \text{ s}^{-1}$  and  $g = 9.8 \text{ m s}^{-2}$ .

	$L_0$	$u'$	$Re_\lambda$	$\tau_{\text{eddy}}$	$\tau_\eta$	$\eta$	$u_\eta$	$Re_b$	$R_0/\eta$	$St$	$g\tau_b/u_\eta$
(a')	5.0	1.4	94	3.6	0.093	0.025	0.275	1.0	1.13	0.14	0.55
(b')	5.0	1.0	87	4.9	0.147	0.032	0.218	1.0	0.89	0.09	0.69
	$L_0$ (cm)	$u'$ (cm/s)	$Re_\lambda$	$\tau_{\text{eddy}}$ (ms)	$\tau_\eta$ (ms)	$\eta$ ( $\mu\text{m}$ )	$u_\eta$ (cm/s)	$Re_b$	$R_0/\eta$	$St$	$g\tau_b/u_\eta$
(a')	0.41	7.2	94	57.3	4.7	68.7	1.45	1.0	1.13	0.14	0.55
(b')	0.46	5.5	87	82.5	7.3	85.7	1.16	1.0	0.89	0.09	0.69

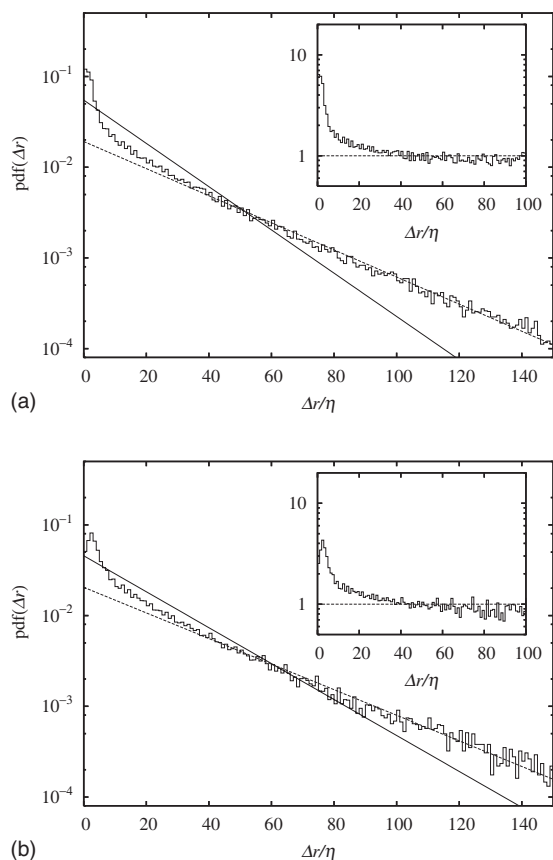


FIG. 3. Numerical result on the probability density function of distance between successive bubbles,  $\text{pdf}(\Delta r)$ . Case (a') (top) is the most turbulent. In the inset, the same compensated plot as in Fig. 1.

ness of Fig. 4, where departure from the Poisson scaling already starts below  $\eta$  scale. Second, the most turbulent case is the most clustered, (a') ( $\text{Re}_\lambda \approx 94$ ) more than (b') ( $\text{Re}_\lambda \approx 87$ ). The evaluation of the fraction of clustered bubbles, based on the fit of the  $\text{pdf}(\Delta r)$  as in the experiment, gives the value 29% for (a') and 37% for (b'). Though the qualitative behavior of the statistical indicators is the same, also some important differences arise in this comparison. First of all, full homogeneity in the numerics seems to be recovered already at scales of order  $\mathcal{O}(10\eta)$ , whereas in the experiments it was only recovered at  $\mathcal{O}(100\eta)$ . Furthermore, the deviations from the Poisson distribution and the fraction of clustered bubbles are definitely stronger in the numerics. There are several possible interpretation for this mismatch, including the possible incompleteness of the employed model Eq. (1): first, some physical effects have been neglected: the fluid-bubble and the bubble-bubble couplings and the associated finite-size effects (in the present conditions bubbles can overlap!). A second reason can be the different degree of bubble interaction with turbulence, a quantity that is parametrized by the Stokes number  $\text{St} = \tau_b / \tau_\eta$ . The estimated  $\text{St}$  in the experiment is roughly one order of magnitude smaller than in the simulation. This corresponds to bubbles that react faster to the fluid velocity changes and hence to bubbles that closely follow the fluid particles and accumulate less. Such a trend is also confirmed by our numerics.

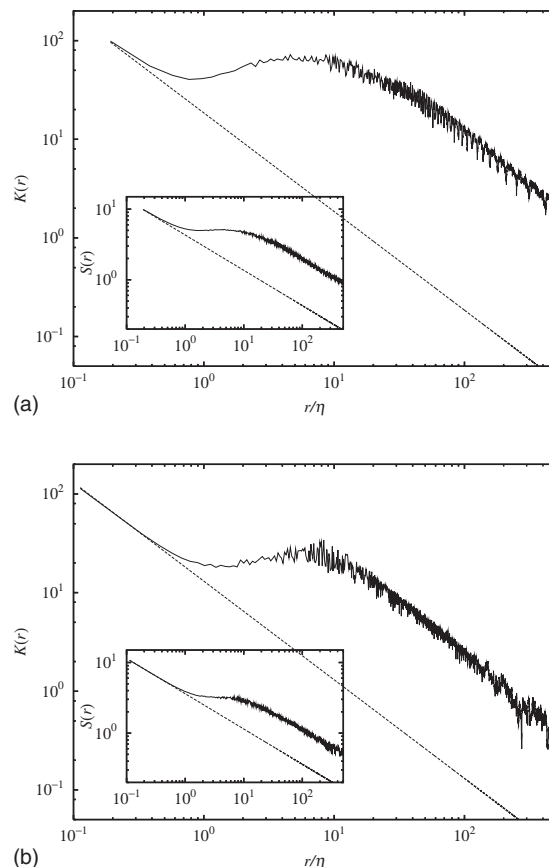


FIG. 4. Numerical result on scale dependent kurtosis,  $K(r)$ , for case (a') (top) and (b') (bottom), and Poissonian behavior (dotted). In the insets, the scale dependent skewness,  $S(r)$ , behavior is shown.

## VI. CONCLUSIONS

We have performed statistical tests in order to detect and quantitatively characterize the phenomenon of preferential bubble concentration from single-point hot-wire anemometer measurements in the bulk of a turbulent channel. Our tools clearly show that the experimental records display bubble clustering. The fraction of bubbles trapped in such structures is indeed considerable and can be estimated to be of the order of 10%. The scale dependent deviations from random-homogeneous distribution, that we associate to typical cluster dimension, extends from the smallest detectable scale,  $\mathcal{O}(\eta)$ , to scales in the low inertial range,  $\mathcal{O}(100\eta)$ . Accumulation of bubbles is enhanced by increasing the turbulence intensity. Comparison with present Eulerian-Lagrangian simulations, where pointlike bubbles strongly accumulate in vortex core regions, shows similar qualitative features and trends.

We hope that our explorative investigation will stimulate new dedicated experiments and numerical simulations to further quantify the clustering dynamics as function of Reynolds number and particle size, type, and concentration. The challenge is to further develop and employ quantitative statistical tools to allow for a meaningful comparison between experiment and simulations, in order to validate the modeling of particles and bubbles in turbulent flow.

## ACKNOWLEDGMENTS

We thank Stefan Luther and GertWim Bruggert for extensive help with the experimental setup and the measurements, and for useful discussions. We are grateful to Kazuyasu Sugiyama for useful remarks. This work is part of the research program of the Stichting voor Fundamenteel Onderzoek der Materie FOM, which is financially supported by the Nederlandse Organisatie voor Wetenschappelijk Onderzoek NWO.

- <sup>1</sup>J. Fessler, J. Kulick, and J. Eaton, "Preferential concentration of heavy particles in a turbulent channel flow," *Phys. Fluids* **6**, 3742 (1994).
- <sup>2</sup>S. Douady, Y. Couder, and M. E. Brachet, "Direct observation of the intermittency of intense vorticity filaments in turbulence," *Phys. Rev. Lett.* **67**, 983 (1991).
- <sup>3</sup>G. P. Bewley, D. P. Lathrop, and K. R. Sreenivasan, "Superfluid helium—Visualization of quantized vortices," *Nature (London)* **441**, 588 (2006).
- <sup>4</sup>M. Bourgoïn, N. T. Ouellette, H. T. Xu, J. Berg, and E. Bodenschatz, "The role of pair dispersion in turbulent flow," *Science* **311**, 835 (2006).
- <sup>5</sup>K. Hoyer, M. Holzner, B. Luethi, M. Guala, A. Lieberzon, and W. Kinzelback, "3D scanning particle tracking velocimetry," *Exp. Fluids* **39**, 923 (2005).
- <sup>6</sup>S. Ayyalasomayajula, A. Gylfason, L. R. Collins, E. Bodenschatz, and Z. Warhaft, "Lagrangian measurements of inertial particle accelerations in grid generated wind tunnel turbulence," *Phys. Rev. Lett.* **97**, 144507 (2006).
- <sup>7</sup>C. T. Crowe, T. Troutt, and J. N. Chung, "Numerical models for two-phase turbulent flows," *Annu. Rev. Fluid Mech.* **28**, 11 (1996).
- <sup>8</sup>M. R. Maxey, "The gravitational settling of aerosol particles in homogeneous turbulence and random flow fields," *J. Fluid Mech.* **174**, 441 (1987).
- <sup>9</sup>K. Squires and J. Eaton, "Preferential concentration of particles by turbulence," *Phys. Fluids A* **3**, 1169 (1991).
- <sup>10</sup>L. Wang and M. Maxey, "Settling velocity and concentration distribution of heavy particles in homogeneous isotropic turbulence," *J. Fluid Mech.* **256**, 27 (1993).
- <sup>11</sup>J. Bec, L. Biferale, G. Boffetta, A. Celani, M. Cencini, A. Lanotte, S. Musacchio, and F. Toschi, "Acceleration statistics of heavy particles in turbulence," *J. Fluid Mech.* **550**, 349 (2006).
- <sup>12</sup>S. Elghobashi and G. Truesdell, "On the two-way interaction between homogeneous turbulence and dispersed solid particles. I: Turbulence modification," *Phys. Fluids A* **5**, 1790 (1993).
- <sup>13</sup>I. Mazzitelli, D. Lohse, and F. Toschi, "The effect of microbubbles on developed turbulence," *Phys. Fluids* **15**, L5 (2003).
- <sup>14</sup>I. Mazzitelli, D. Lohse, and F. Toschi, "On the relevance of the lift force in bubbly turbulence," *J. Fluid Mech.* **488**, 283 (2003).
- <sup>15</sup>S. Elghobashi and G. Truesdell, "Direct simulation of particle dispersion in a decaying isotropic turbulence," *J. Fluid Mech.* **242**, 655 (1992).
- <sup>16</sup>L. Biferale, G. Boffetta, A. Celani, A. Lanotte, and F. Toschi, "Particle trapping in three-dimensional fully developed turbulence," *Phys. Fluids* **17**, 021701 (2005).
- <sup>17</sup>J. Chun, D. L. Koch, S. L. Rani, A. Ahluwalia, and L. R. Collins, "Clustering of aerosol particles in isotropic turbulence," *J. Fluid Mech.* **536**, 219 (2005).
- <sup>18</sup>We have recently studied preferential concentration in E. Calzavarini, M. Kerscher, D. Lohse, and F. Toschi, *Dimensionality and morphology of particle and bubble clusters in turbulent flow*, *J. Fluid Mech.* (to be published), see arXiv:0710.1705.
- <sup>19</sup>G. Falkovich and A. Pumir, "Intermittent distribution of heavy particles in a turbulent flow," *Phys. Fluids* **16**, L47 (2004).
- <sup>20</sup>T. H. van den Berg, S. Luther, I. Mazzitelli, J. Rensen, F. Toschi, and D. Lohse, "Bubbly turbulence," *J. Turbul.* **7**, 1 (2006).
- <sup>21</sup>L. Wang and M. Maxey, "The motion of microbubbles in a forced isotropic and homogeneous turbulence," *Appl. Sci. Res.* **51**, 291 (1993).
- <sup>22</sup>J. M. Rensen, S. Luther, and D. Lohse, "Velocity structure functions in turbulent two-phase flows," *J. Fluid Mech.* **538**, 153 (2005).
- <sup>23</sup>T. van den Berg, S. Luther, and D. Lohse, "Energy spectra in microbubbly turbulence," *Phys. Fluids* **18**, 038103 (2006).
- <sup>24</sup>M. Lance and J. Bataille, "Turbulence in the liquid phase of a uniform bubbly air-water flow," *J. Fluid Mech.* **222**, 95 (1991).
- <sup>25</sup>S. Luther, J. Rensen, T. van den Berg, and D. Lohse, "Data analysis for hot-film anemometry in turbulent bubbly flow," *Exp. Therm. Fluid Sci.* **29**, 821 (2005).
- <sup>26</sup>J. M. Rensen, S. Luther, J. de Vries, and D. Lohse, "Hot-film anemometry in bubbly flow I: Bubble-probe interaction," *Int. J. Multiphase Flow* **31**, 285 (2005).
- <sup>27</sup>T. Bergenblock, F. Onofri, B. Leckner, and L. Tadriss, "Experimental estimation of particle flow fluctuations in dense unsteady two-phase flow using phase Doppler anemometry," *Int. J. Multiphase Flow* **33**, 849 (2007).
- <sup>28</sup>R. Zenit, D. Koch, and A. Sangani, "Measurements of the average properties of a suspension of bubbles rising in a vertical channel," *J. Fluid Mech.* **429**, 307 (2001).
- <sup>29</sup>W. Feller, *An Introduction to Probability Theory and Its Applications* (Wiley, New York, 1968).
- <sup>30</sup>M. Maxey and J. Riley, "Equation of motion for a small rigid sphere in a nonuniform flow," *Phys. Fluids* **26**, 883 (1983).